Supporting Information

Cobalt (II) Monoxide Nanoparticles Embedded in Porous Carbon Nanofibers as a Highly Reversible Conversion Reaction Anode for Li-ion Batteries

Won-Hee Ryu[a], Jungwoo Shin[a], Ji-Won Jung[a] and Il-Doo Kim[a,b]*

[a] Department of Materials Science and Engineering, Korea Advanced Institute of Science and Technology (KAIST), 291 Daehak-ro, Yuseong-gu, Daejeon 305-701, Korea

[b] KAIST Institute for the NanoCentury, Korea Advanced Institute of Science and Technology, Daejeon 305-701, Republic of Korea

Experimental details

Synthesis of CoO nanoparticle embedded carbon nanofibers

Cobalt (II) acetate anhydrous ($CoC_4H_6O_4$,99.995%, Sigma–Aldrich Co., Ltd., USA), Polyacrylonitrile (PAN, Mw = 150,000, Sigma–Aldrich Co., Ltd., USA), and N, N dimethylformamide (99.8%, Sigma–Aldrich Co., Ltd., USA) were purchased and used without any purification. To prepare a metal precursor solution, 0.2 g of $CoC_4H_6O_4$ was dissolved in 3 g of N, N dimethylformamide, and continuously stirred at the room temperature (RT) for 6 h. PAN was separately dissolved in 5 g of N , N dimethylformamide, and continuously stirred at 80 °C for 3 h. Each metal precursor and PAN solutions were subsequently mixed each other for 2 h. For comparison, sole PAN solution was prepared by dissolving the PAN (0.5 g) in the 4 g of N, N dimethylformamide. A feeding rate was controlled to be 0.5 ml/h during electrospinning and a stainless steel foil as a collector was vertically positioned at 20 cm away from the syringe needle (25 gauge) under a constant potential of 12 kV to collect as-spun Co precursor/PAN nanofibers. The obtained as-spun nanofibers were stabilized at 280 °C for 1 h. in the air atmosphere, and subsequently carbonized at 700 °C for 1 h. under the inert Ar atmosphere. The unique nanostructure composed with both CoO and carbon nanofiber can be maintained by proper heat treating time under the inert Ar atmosphere. Under too reductive condition for heat treatment, CoO phase tend to turn into metallic cobalt phase. On the other hands, CNF backbone is easily reacted with oxygen, and then is fully evaporated as CO_x gas under the too oxidative condition. The morphologies of the prepared samples were observed by scanning electron microscopy (SEM, PHILIPS, XL30SFEG) and transmission

electron microscope (TEM, FEI, Tecnai F30 S-Twin). The exact weight percent of carbon in the samples was confirmed by element analyzer (EA). The crystalline phase of the samples was analyzed by X-ray diffraction (XRD, RIGAKU, D/MAX-RC) and X-ray photoelectron spectroscopy (XPS, Thermo, MultiLab 2000).

Electrochemical characterization

Electrochemical performance of the pure CNF and CoO nanoparticle embedded CNF was evaluated in coin-type cells (2032, Hohsen). The anode was fabricated by casting a slurry, consisting of 80 wt% of active material (Both CoO and CNF are considered as active materials), 5 wt% of super P, and 15 wt% of polyvinylidene difluoride (PVDF) binder in N-methyl-2-pyrrolidone (NMP), on a copper foil. The average loading density of the active materials was 0.5 mg/cm^2. A Li-metal foil was used as the counter electrode and 1 M LiPF$_6$ in a 1:1 mixture (by volume) of ethylene carbonate: diethylene carbonate (Soulbrain Co., Ltd., Korea) was used as the electrolyte. The separator was a Celgard 2325 (25 μm thick). The cells were galvanostatically charged and discharged between 0.01 and 3.0 V (vs. Li/Li$^+$) at various currents. All of the potentials refer to Li/Li$^+$.

To help understand the synthetic procedure of CoO nanoparticle embedding in CNF, a schematic illustration was provided in Fig. S1, summarizing the steps of the experiment.
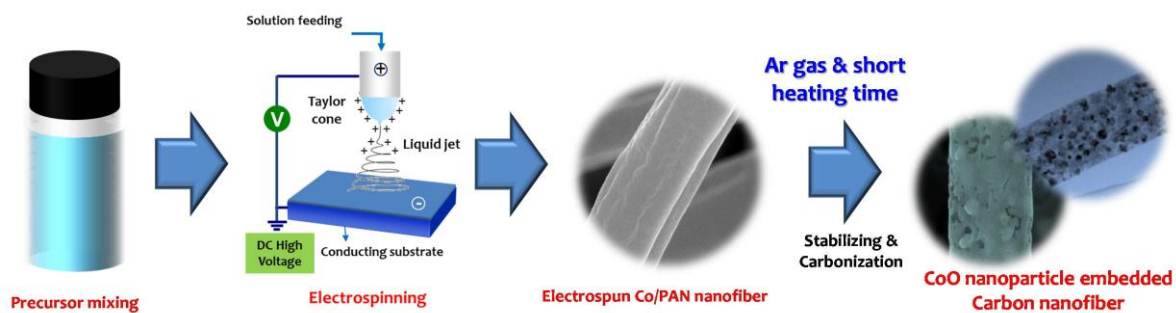
Fig. S1. Schematic illustration of the synthetic procedure of CoO nanoparticle embedded in CNF.

Fig. S2 shows SEM images of as-spun Co precursor/PAN composite fibers with different levels of magnification. The continuous and uniform as-spun fibers have smooth surfaces with an average diameter of 640 nm.
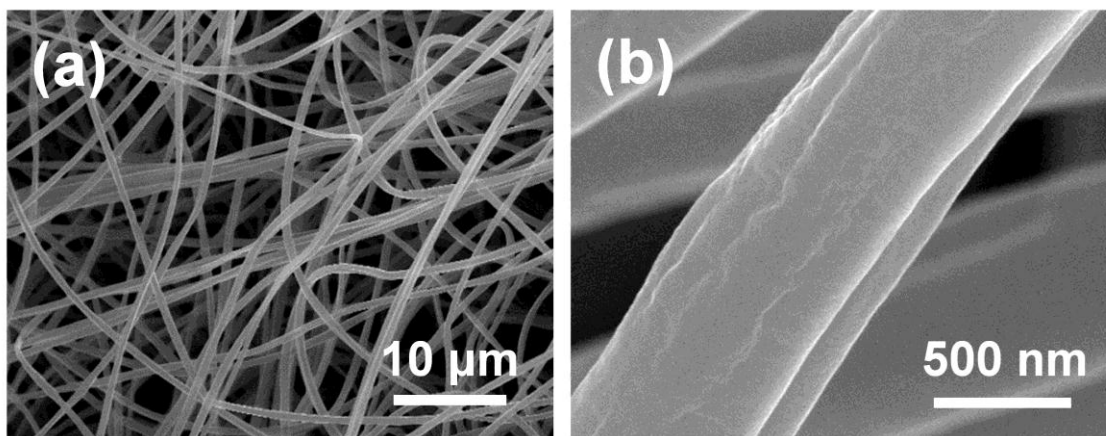
Fig. S2. SEM images of as-spun NFs of Co precursor with PAN polymer prepared by electrospinning with different levels of magnification.

Fig. S3 shows SEM images of pristine CNFs with different magnifications. A smooth surface without any pores was found in the pristine CNFs, compared to the case of CoO embedded CNFs, which have many pores on the surface. The average diameter of CNFs was estimated to be 450 nm.
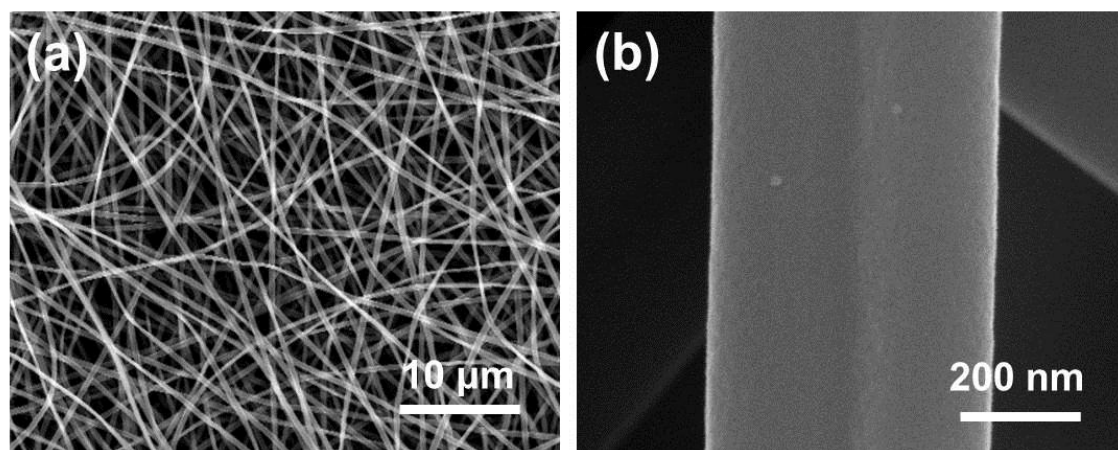
Fig. S3. SEM images of pristine CNFs prepared by electrospinning with different magnifications.

Fig. S4 shows the X-ray diffraction patterns (XRD) and X-ray photoelectron spectroscopy (XPS) results. Fig. S4a indicate that the nanoparticles are consisted of cobalt (II) monoxide phase with weak crystallinity without any other impurity phase. On the other hands, when increasing the loading amount of Co precursor, the phase of metallic Co was dominantly formed and coexisted with CoO phase. That is, excessive loading of Co source in electrospinning solution leads to the formation of Co rather than CoO phase during the calcination under the inert atmosphere. Therefore, the control of critical Co loading amount is important to synthesize single phase CoO which is embedded in the CNFs. In order to clearly confirm the crystalline phase and the oxidation states of the CoO nanoparticles, we carried out X-ray photoelectron spectroscopy (XPS) analysis (Fig. S4b). From the XPS spectra of Co 2p core level, the peak at 780.4 eV for $2p_{3/2}$ is corresponds to the shakeup satellite peak at 786.7 for $2p_{3/2}$, while the peak at 796.2eV for $2p_{1/2}$ is attributed to the shakeup satellite peak at 802.5 eV for $2p_{1/2}$. The presence of both peaks at 780.4 and 796.2 eV and their obvious satellite peaks indicates that the oxidation number of Co ions is +2. In addition, the peak at 778.1 eV corresponding to the impurity phase of Co^0 metal was not observed in the CoO embedded CNF.
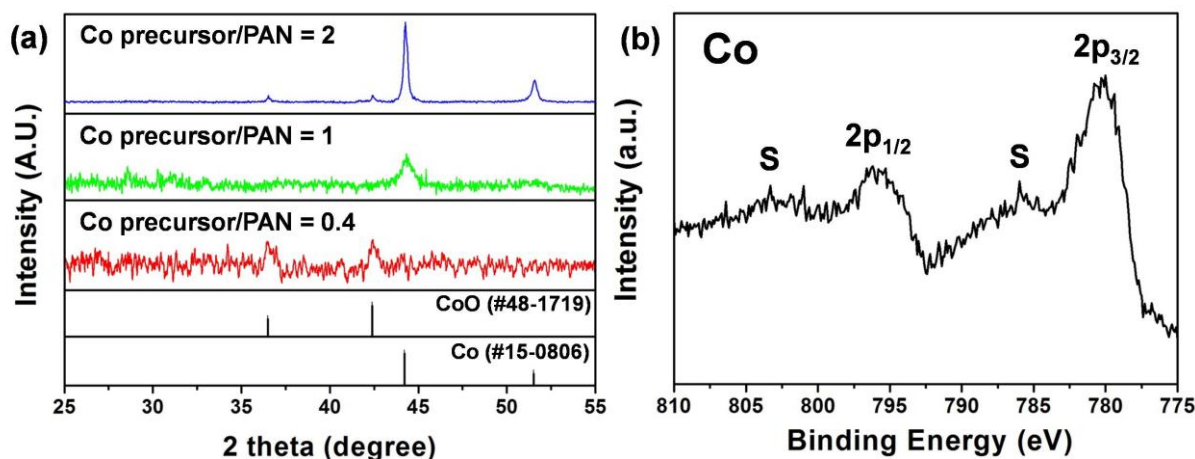
Fig. S4 (a) X-ray diffraction patterns of Co/CoO nanoparticles embedded in CNFs calcined at 700 °C under Ar atmosphere with different ratios of Co precursor/PAN: 0.4, 1 and 2. (b) X-ray photoelectron spectra collected from Co 2p of CoO embedded CNF prepared with 0.4 of Co precursor/PAN ratio (Co precursor: 0.2 g).

Fig. S5 shows atomic distributions of O as well as Co and C in nanofiber which was confirmed by TEM-EDS mapping. The atomic distribution of Co was increased with increasing the ratio of Co source/PAN from 0.4 to 2. In case of high Co source (Co precursor/PAN: 2), metallic Co species were extensively distributed and coarsened in the most of area in the nanofiber. Atomic distribution of O in the fiber indicates the existence of CoO phase. However, the atomic distribution of O was relatively blurred because of weak crystallinity of CoO.
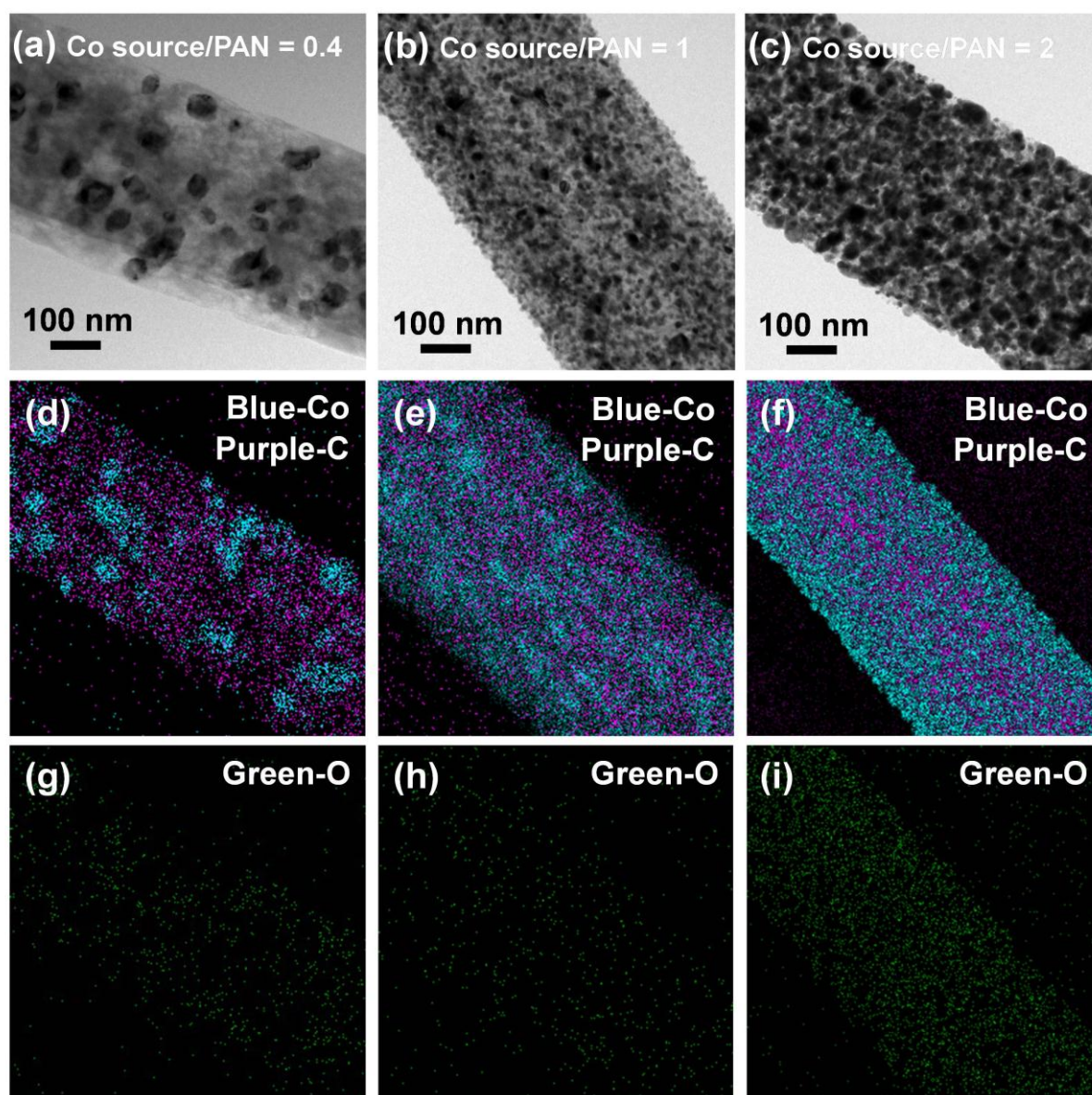
Fig. S5 (a) STEM images of Co/CoO nanoparticles embedded in CNFs calcined with different ratios of Co precursor/PAN; (a) 0.4 (Co precursor: 0.2 g), (b) 1 (Co precursor: 0.5 g) and (c) 2 (Co precursor: 1 g); atomic distribution of Co (blue color) and C (purple color) analyzed from STEM images of (a), (b) and (c), respectively; (d) 0.4 (e) 1 and (f) 2; atomic distribution of O (green color) analyzed from STEM images of (a), (b) and (c), respectively; (g) 0.4 (h) 1 and (i) 2.
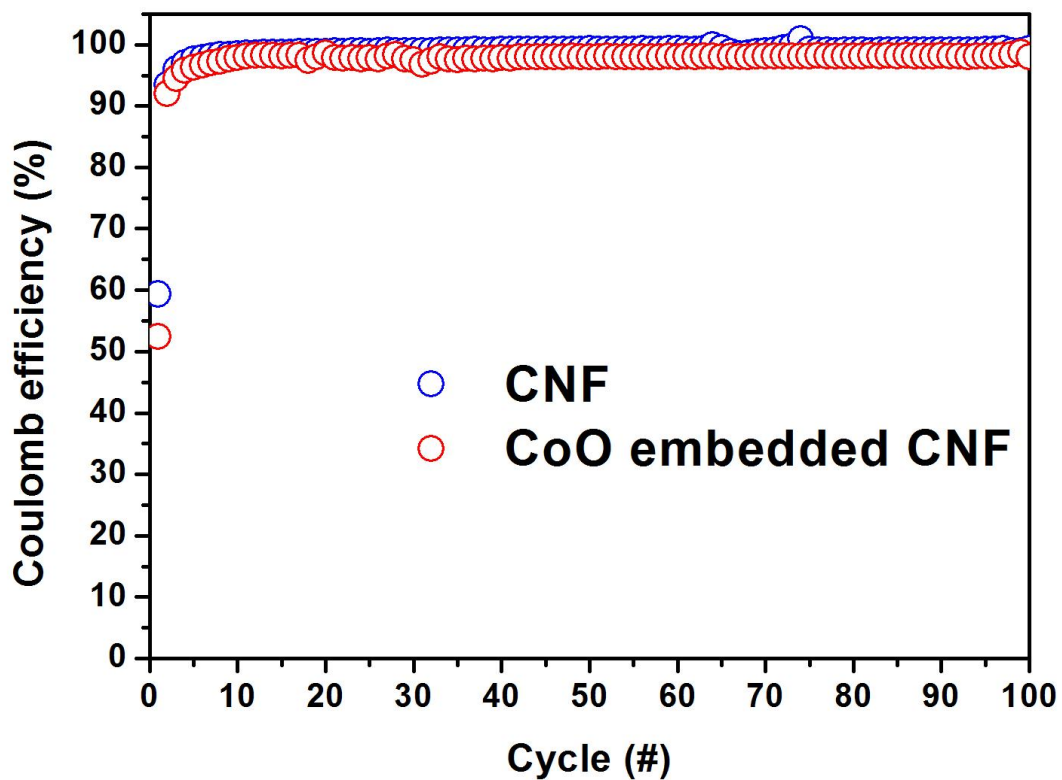
Fig. S6 Coulomb efficiency of the CNF and CoO embedded CNF for 100 cycles

Fig. S7 shows the *ex-situ* XRD results of the CoO embedded CNF electrode after the 1st discharge and the subsequent 1st charge, corresponding to Fig. 3c and 3d, respectively. From the *ex-situ* XRD results, the poorly crystalline CoO phase was found to have completely decomposed after the initial discharge, giving an amorphous-like phase. The Co phase after the 1st discharge and the CoO phase recovered after the subsequent 1st charge were not confirmed by *ex-situ* XRD. Therefore, we carefully confirmed the reversible conversion reaction of CoO phase (CoO + 2Li$^+$ + 2e $\leftrightarrow$ Li$_2$O + Co) by *ex-situ* TEM analysis (Fig. 3).
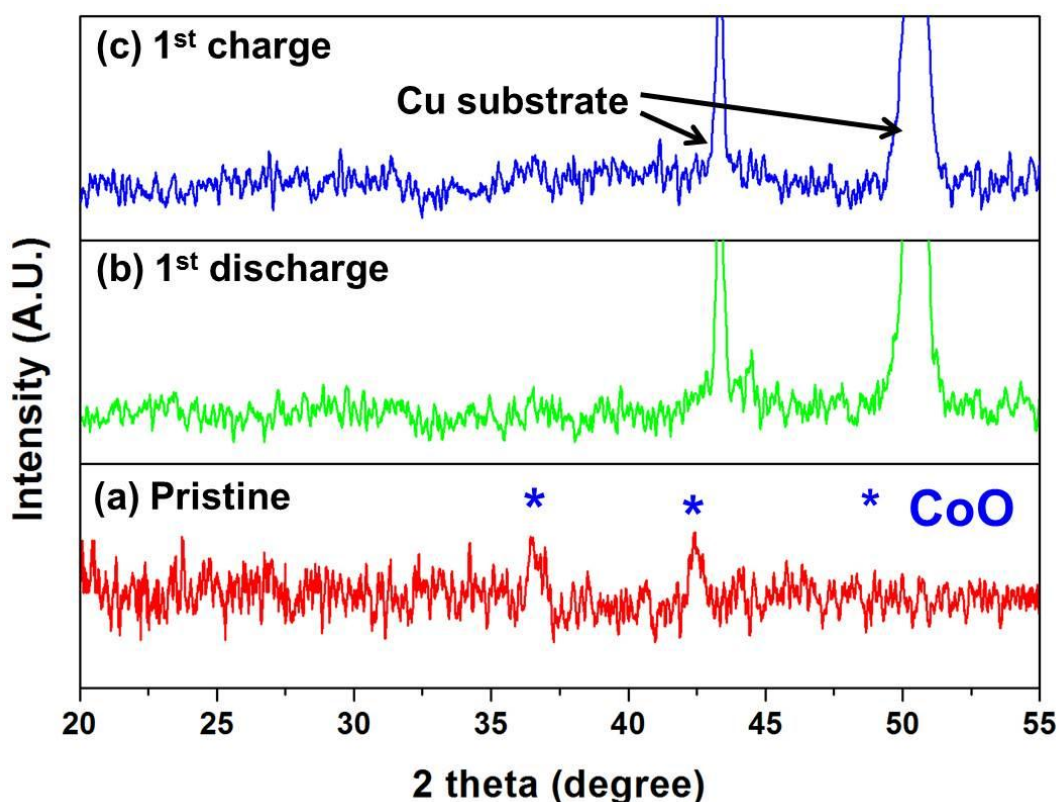
Fig. S7. X-ray diffraction patterns of CoO embedded CNF collected at various points along the charging/discharging state.

Fig. S8 shows the charge/discharge curves of pristine CNFs and CoO-embedded CNF during the initial three cycles and at the 100th cycle. In the case of the CoO-embedded CNF, a gradual increase of the capacity during 100 cycles was observed. The CoO nanoparticles which were positioned in the inner core of the CNF may not have been fully activated in the initial charging/discharging reaction. When cycling proceeded, the residual CoO nanoparticles may have participated further in the electrochemical reaction with the Li ions. However, there is no significant difference in the charge and discharging curves between the second and third cycles after the first cycle and the 100th cycle and no additional plateau, indicating that the conversion reaction of the CoO-embedded CNF was well maintained during the long cycling process without a phase change.
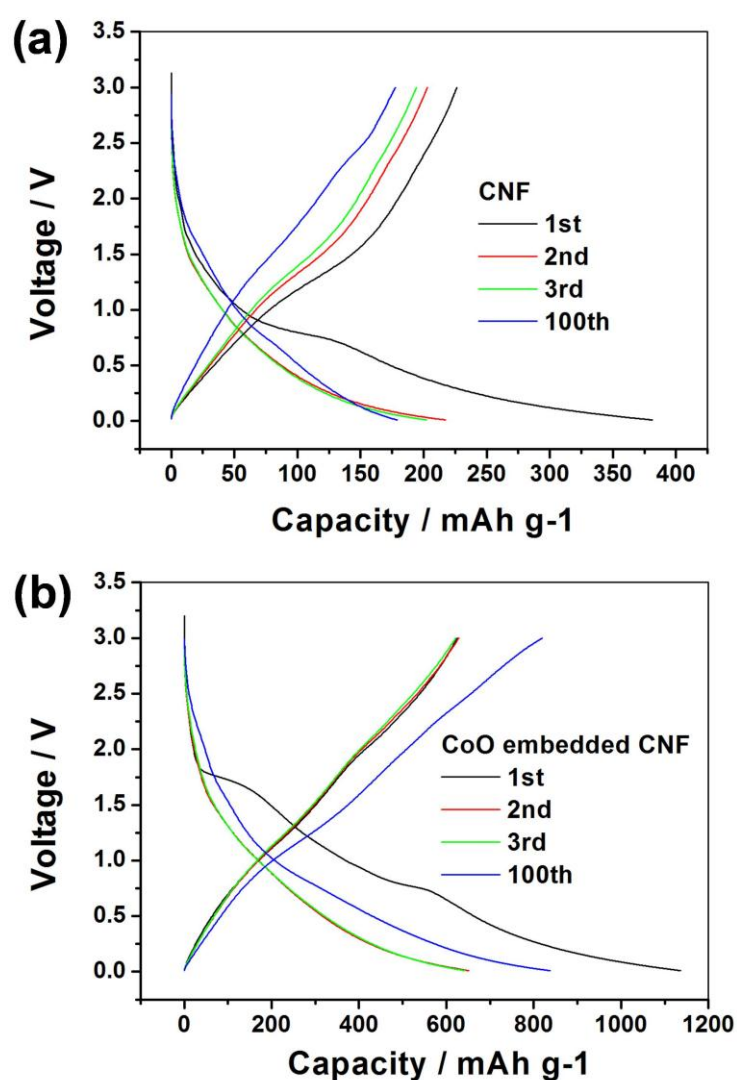
Fig. S8. Charge/discharge curves of (a) pristine CNFs and (b) CoO-embedded CNF during the initial three cycles and at the 100th cycle.

Amount of Co precusor (g)	Co (At%)	O (At%)	C (At%)	C (wt%) obtained from EA
0.2	8.8	8.67	82.53	51
0.5	12.4	6.81	80.79	30.9
1	19.2	8.49	72.31	19.3

Table S1. Atomic percentage of Co, O, and C (EDS) and weight percentage of C (EA) in the Co/CoO embedded CNF synthesized at different amount of Co precorsor.